





Article

Experimental Study of Electrical Properties of Pharmaceutical Materials by Electrical Impedance Spectroscopy

Manuel Vázquez-Nambo ¹, José-Antonio Gutiérrez-Gnecchi ^{1,*}, Enrique Reyes-Archundia ¹ ,
Wuqiang Yang ² , Marco-A. Rodríguez-Frias ², Juan-Carlos Olivares-Rojas ¹  and
Daniel Lorias-Espinoza ³ 

¹ Tecnológico Nacional de México/Instituto Tecnológico de Morelia, División de Estudios de Posgrado E Investigación, Avenida Tecnológico 1500, Morelia C. P 58120, Michoacán, Mexico; manuelvn02@gmail.com (M.V.-N.); reyes_archundia@yahoo.com.mx (E.R.-A.); jcolivares@itmorelia.edu.mx (J.-C.O.-R.)

² Department of Electrical and Electronic Engineering, The University of Manchester, Manchester M13 9PL, UK; wuqiang.yang@manchester.ac.uk (W.Y.); marco.rodriguezfrías@manchester.ac.uk (M.-A.R.-F.)

³ CINVESTAV/IPN, Av. Instituto Politécnico Nacional 2508, Col. San Pedro Zacatenco, México C.P 07360, D. F., Mexico; dlorias@cinvestav.mx

* Correspondence: bionsprocessing@aol.com; Tel.: +52-44-33-12-15-70

Received: 10 July 2020; Accepted: 15 September 2020; Published: 21 September 2020



Abstract: The physicochemical characterization of pharmaceutical materials is essential for drug discovery, development and evaluation, and for understanding and predicting their interaction with physiological systems. Amongst many measurement techniques for spectroscopic characterization of pharmaceutical materials, Electrical Impedance Spectroscopy (EIS) is powerful as it can be used to model the electrical properties of pure substances and compounds in correlation with specific chemical composition. In particular, the accurate measurement of specific properties of drugs is important for evaluating physiological interaction. The electrochemical modelling of compounds is usually carried out using spectral impedance data over a wide frequency range, to fit a predetermined model of an equivalent electrochemical cell. This paper presents experimental results by EIS analysis of four drug formulations (trimethoprim/sulfamethoxazole $C_{14}H_{18}N_4O_3$ - $C_{10}H_{11}N_3O_3$, ambroxol $C_{13}H_{18}Br_2N_2O.HCl$, metamizole sodium $C_{13}H_{16}N_3NaO_4S$, and ranitidine $C_{13}H_{22}N_4O_3S.HCl$). A wide frequency range from 20 Hz to 30 MHz is used to evaluate system identification techniques using EIS data and to obtain process models. The results suggest that arrays of linear R-C models derived using system identification techniques in the frequency domain can be used to identify different compounds.

Keywords: drug modelling; frequency response; electrical impedance spectroscopy; system identification

1. Introduction

In pharmaceutical research, analytical science plays an essential role in the physicochemical characterization of properties of drug materials, intermediates, drug products, drug formulation, impurity, degradation products, and biological samples containing the drugs and their metabolites [1]. Amongst many analytical spectroscopic measurement techniques, Electrical Impedance Spectroscopy (EIS) is simple and cost-effective for elucidating a wide range of electrophysical properties ranging from bioanalytical to biological and food characterization [2,3]. However, EIS can only analyse properties of bulk material as a whole, unlike other spectroscopy methods, by which individual chemical species can

be determined. Thus, a number of factors, such as the measurement method, the experimental setup (including electrode array, test cell, and environmental conditions) and analytical development of resulting models, can influence the quality of measured data and information obtained. The importance of using EIS information for electrochemical cell characterization drives the continuous report of novel mathematical methods as well as the introduction of experimental and commercial software solutions that allow for the tailoring of specific models to particular electrochemical cell arrays, based on frequency-domain experimental data. However, there are still challenges to overcome, in particular, accounting for the non-stationary nature of electrochemical cells. Ragoisha [4] addresses some of these challenges, and, amongst various aspects, discusses the importance of considering multidimensional, non-stationary EIS information towards a universal electrochemical response analyser that bridges the gap between DC, single-frequency AC and EIS methods.

For instance, targeted drug delivery is a typical example of a dynamic, multidimensional process where the use of EIS measurements can have important implications for real-time analysis of drug dispersion dynamics towards improving the effectiveness of medical treatments. Rimpiläinen et al. [5] demonstrated that Electrical Impedance Tomography can be used for imaging changes in concentration of propranolol hydrochloride, dissolving ad hoc tablets in salty liquid media using a test phantom fitted with five 16-electrode measurement planes. On the other hand, different tissues exhibit different electrical impedance properties as a function of frequency (Gabriel et al. [6–8]), and thus EIS can be used to distinguish different tissues. However, drug delivery alters the electrical properties of the tissue [9], and thus it is necessary to develop methods that can lead to the real-time identification of different components. Therefore, there are incentives to further develop electrical impedance analysis methods that can provide a mathematical model, suitable for determining the electrical properties of dynamic systems and can also provide a mathematical score of the feasibility of the model so as to represent the electrochemical cell processes. Here, the authors focus on developing the procedure based on frequency-domain system identification methods to analyse the frequency response of the electrochemical cell that can be recalculated from frequency-domain response data, required for reproducible and precise identification and quantification of drug analysis as they are essential in discovery, development, and evaluation of drugs.

2. Materials and Methods

2.1. Frequency Response Measurement Methods

Amongst the electro-analytical techniques used for measuring the transport properties of ions in solutions, cyclic voltammetry (CV) and galvanostatic charge–discharge (GCD) methods are commonly used for modelling the impedance of electrochemical cells, which in turn can be correlated to various properties of the cell array and bulk solution. CV requires controlling the excitation voltage while measuring the resulting current. GCD requires applying a controlled current and measuring the resulting potential. Recently, new EIS data acquisition systems were proposed to improve automated data acquisition. For instance, Grossi et al. developed a low-cost portable measurement system based on a microcontroller to obtain an EIS spectrum of four saline solutions (NaCl, Na₂CO₃, K₂HPO₄ and CuSO₄) in a frequency range from 10 Hz up to 10 kHz. [10]; the excitation signal (i.e., a sinewave) is generated by an AD5932 function generator so that the frequency response measurement can be approximated to the test solution. Therefore, the choice of the measurement method is a compromise, with the following four considerations.

- (1) The frequency measurement range should be suitable for capturing the frequency response of the process accurately over a high-frequency range (Figure 1).
- (2) The measurement method should provide an accurate impedance measurement over the entire frequency measurement range.
- (3) The method should require minimal calibration procedure.
- (4) The measurement method must be suitable for measuring the properties of the test bulk material.

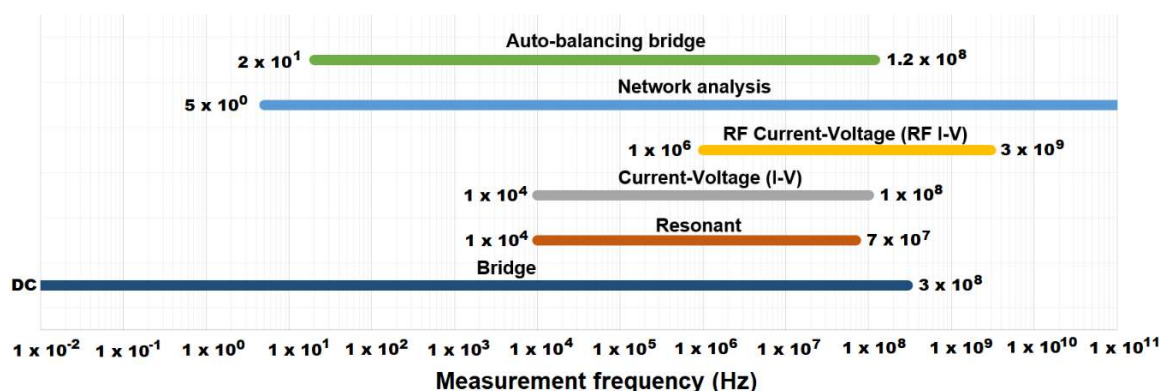


Figure 1. Frequency measurement range of six common impedance measurement methods [11]. Authors' graphical summary extracted from product information. Reproduced with permission, courtesy of ©Keysight Technologies, Inc., 2009–2016.

Therefore, the choice of the measurement method is essential to ensure the quality of measured data, as well as the reproducibility of results. Table 1 lists available measurement methods. Ultimately, efforts are made towards developing measurement solutions to obtaining a fingerprint frequency response of the test sample [10].

2.2. Sensing Electrode Array

Characterization of the physicochemical properties of bulk materials has spearheaded the application of EIS in many areas to study the effect of electrode shape, size and material on electrode–solution interaction. Since Newman studied the influence of electrode geometry on current distribution continuity to understand frequency dispersion processes [12–15], significant advances are continually reported in developing sensing electrodes to understand the correlation of different compounds in bulk solutions with frequency response to identify and quantify the presence of particular substances. Levent et al. demonstrated that a boron-doped diamond electrode can detect amroxol in concentrations of 0.05–0.7 μM [16]. Yari and Shams presented a silver-filled multi-walled carbon nanotube for determination of sulfamethoxazole, in the range 0.05–70 μM , in pharmaceutical formulations and urine [17]. Sgobbi et al. developed a screen-printed electrochemical sensor for the detection of sulfamethoxazole and trimethoprim without pre-treating the sample [18]. Recently, Chen et al. presented a graphene-based electrode for the determination of sulfamethoxazole in aqueous environments [19].

Despite the fact that improved measurement technologies, including electrode sensing technologies, are continuously introduced, and the experimental setup may be relatively simple (i.e., bulk solution in the presence of a set of electrodes), the process of modelling electrical properties of bulk solutions is by no means complex because there are many physicochemical processes involved.

Table 1. Common impedance measurement methods [11]. Reproduced with permission, courtesy of ©Keysight Technologies, Inc., 2009–2016.

Measurement Method	Advantages	Disadvantages	Applicable Frequency Range	Applications
Bridge	High accuracy (0.1% typically) Wide frequency range coverage by using different types of bridges Low Cost	Needs to be manually balanced Narrow frequency coverage with a single instrument	DC to 300 MHz	Standard Lab
Resonant method	Good Q accuracy up to high Q	Needs to be tuned to resonance Low impedance measurement accuracy	10 kHz to 70 MHz	High-Q device measurement
Current–voltage (I–V)	Grounded device measurement Suitable to probe-type test needs	Operating frequency range is limited by transformer used in probe	10 kHz to 100 MHz	Grounded device measurement
RF I–V	High accuracy (1% typ.) and wide impedance range at high frequencies	Operating frequency range is limited by transformer used in test head	1 MHz to 3 GHz	RF component measurement
Network analysis	Wide frequency coverage from LF to RF Good accuracy when the unknown impedance is close to characteristic impedance	Recalibration required when the measurement frequency is changed Narrow impedance measurement range	5 Hz and above	RF component measurement
Auto-balancing bridge	Wide frequency coverage from LF to HF High accuracy over a wide impedance measurement range Grounded device measurement	High frequency range not available	20 Hz to 120 MHz	Generic component measurement Grounded device measurement

2.3. Basic Electrochemical Electrical Equivalent Circuit (EEC) Models

Physicochemical reactions involve charge transport through the interface and the chemical phases. The kinetics are controlled by charge, mass transfer, or both and depend on the rate at which coupled chemical reactions take place at the electrode-solution interface. In general, a frequency-dependent model can be obtained to fit the impedance data and thus can be correlated with localized physicochemical processes. One of the most common cell models used to correlate basic electrochemical processes to Electrical Impedance Spectroscopy data is the simplified Randles model (also referred to as modified Kelvin–Voigt model) (Figure 2A) which comprises three processes: the solution bulk resistance (i.e., a single resistor, R_B), a polarization resistance, R_P , and a capacitor (C_D) that represents the double layer effect [20].

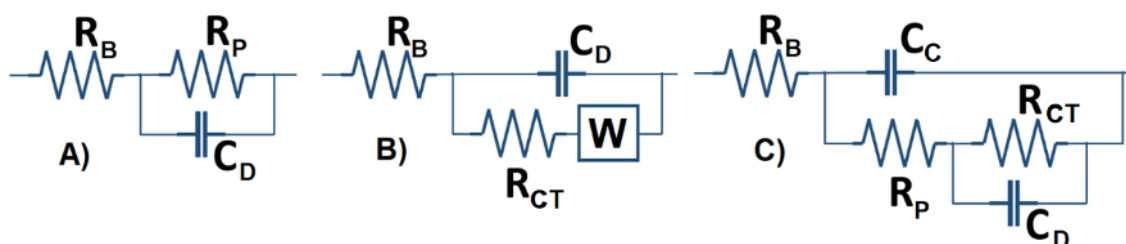


Figure 2. Basic electrochemical electrical equivalent circuit models. (A) Modified Kelvin–Voigt (also known as simplified Randles Model) (B) Randles model and (C) linear approximation of the Randles Model using passive components [20]. Reproduced with permission. © Copyright 1990–2016 Gamry Instruments, Inc.

However, modelling electrochemical dynamic processes often require several additional parameters to be accounted for. For instance, modelling microbial fuel cells involve several processes such as “electrolyte resistance, adsorption of electroactive species, charge transfer at the electrode surface and mass transfer from the bulk solution to the electrode surface” [21].

Thus, a common approach is to combine series and/or parallel arrays of passive components (resistor and capacitors), constant phase elements (CPE) and/or Warburg elements to correlate the measured data with the electrochemical processes involved, including the charge transfer resistance, R_{CT} (Figure 2B) as the interfacial charge transport, mass transfer or both behaviours can explain the interfacial charge transport process and the role of contacts quantitatively by using the electrical equivalent circuit (EEC) [22]. Although the suitability of a measurement model for extracting parameters from EIS experimental data depends on the nature of the electrochemical process, Liao et al. [23] argue that a CPE may not represent distributed-time constant behaviours and therefore the use of a measurement model offers advantages for obtaining low- and high-frequency ohmic resistances. Argawal et al. [24] propose that it is possible to obtain a reasonable approximation fit by selecting the appropriate number of Voigt-type elements; using synthetic data, the authors evaluated the modelling of different processes (CPE, coated materials, diffusion and inductive systems) using the sum of squared errors as a parameter to determine the appropriate number of Voigt-type elements. Thus, it is common to find that CPE and Warburg elements are modelled as combinations on Kelvin–Voigt arrays. For instance, in [20], the authors discuss a simplified model, which considers R_B , R_P , R_{CT} , C_D and the coating capacitance, C_C (Figure 2C).

Tests are also conducted on the bulk solution to determine an appropriate frequency range, where the measured impedance values are best represented. However, different compounds may exhibit great differences over the measurement frequency spectra, and thus, it is necessary to start the modelling process. Software solutions are proposed to facilitate the modelling process [25]. In addition, the measurement range is often constrained up to a few hundred kHz. Nevertheless, it is important to extend the frequency measurement range to capture the frequency response of all processes involved. For instance, in electrochemical systems that exhibit Warburg impedance for a diffusion flux with non-vanishing relaxation, Ramos-Barrado et al. argued that it is necessary to modify the phenomenon-logical description of the electrochemical system in a non-equilibrium state, based on Fickian Diffusion [26]. They further proposed a hyperbolic equation for diffusion flux to explain the prevalence of smaller imaginary values at high frequencies. Huang recently proposed a new impedance expression, which includes three diffusion coefficients (diffusion coefficient of cations, the diffusion coefficient of anions, and the ambipolar diffusion coefficient) to describe the mass transport in electrolytic solutions [27].

Another approach to elucidating system properties is frequency-domain system identification, where a model is estimated from frequency data [28]. Here, we use frequency-domain system identification methods to estimate electrochemical models to differentiate drug compounds.

Modelling electrochemical cells often involve the use of arrays of passive components, resistors and capacitors, where the frequency response data are used to determine the corresponding resistance and capacitance values to fit the frequency response. Similarly, frequency-domain system identification techniques are suited to model RC networks.

2.4. Representation of Basic Kelvin–Voigt Electrochemical Cell Models

In the electrochemical analysis, impedance models are regularly represented in terms of complex variables as a function of the complex term $j\omega$, explicitly, where ω is the frequency in radians per second. In contrast, in control theory and electrical circuit analysis, another approach is to obtain the frequency-domain impedance model of ideal, linear time-invariant passive components in terms of $s = \sigma + j\omega$, through Laplace-Transform. Thus, impedance models of Kelvin–Voigt (parallel) or Maxwell (series) elements can be represented as a function of s . For instance, the equivalent impedance of the Kelvin–Voigt RC parallel network (Figure 3), $Z_{K-V}(s)$, can be represented as a first-order, strictly proper transfer function of s :

$$Z_{K-V}(s) = \frac{R}{sRC + 1} \quad (1)$$

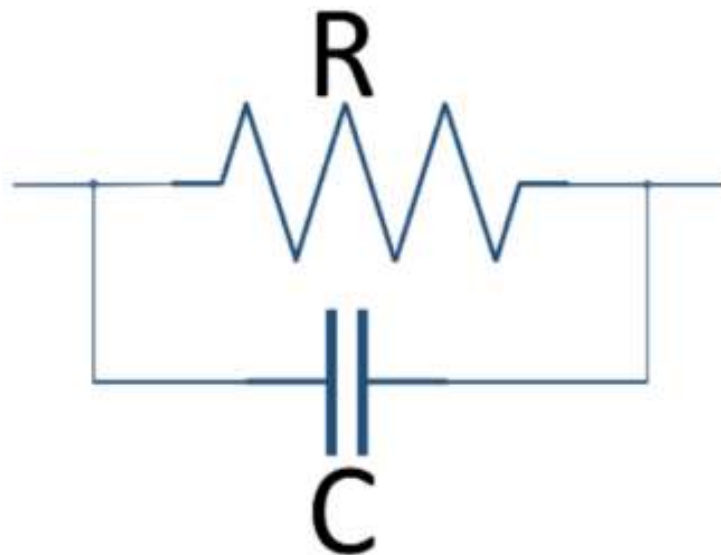


Figure 3. R-C parallel (Kelvin–Voigt type) model.

The equivalent impedance, $Z_{K-V}(s)$, contains a product $RC \equiv \tau$, which is the time constant, and $R \equiv H$, is the system gain when $s \rightarrow 0$ and the root of the denominator (pole) is $(-\frac{1}{\tau})$:

$$Z_{K-V}(s) = \frac{R}{sRC + 1} \equiv \frac{H}{s\tau + 1} \equiv \frac{\left(\frac{H}{\tau}\right)}{s + \left(\frac{1}{\tau}\right)} \quad (2)$$

Introducing a single resistor in series with the R-C parallel array (Figure 4) yields the Modified Kelvin–Voigt element.

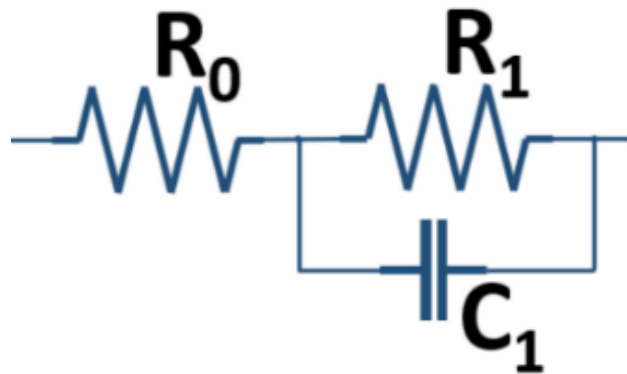


Figure 4. Modified Kelvin–Voigt model.

The impedance of the modified Kelvin–Voigt model, $Z_{MK-V}(s)$, results in a proper polynomial transfer function:

$$Z_{MK-V}(s) = R_0 + \frac{R_1}{sR_1C_1 + 1} = \frac{sR_0R_1C_1 + (R_0 + R_1)}{sR_1C_1 + 1} \tag{3}$$

which can be written in terms of gains and time constants:

$$Z_{MK-V}(s) = R_0 + \frac{R_1}{sR_1C_1 + 1} \equiv H_0 + \frac{H_1}{s\tau + 1} \equiv H_0 + \frac{\left(\frac{H_1}{\tau_1}\right)}{s + \left(\frac{1}{\tau_1}\right)} \tag{4}$$

2.5. State-Space Modelling in the Frequency Domain

Consider the state-space minimal realization of a single-input, single-output (SISO) linear time-invariant system in the frequency domain:

$$G(s) = C(sI - A)^{-1}B + D \tag{5}$$

The state-space frequency-domain system identification problem consists of obtaining a set of parameters $[\hat{A}, \hat{B}, \hat{C}, \hat{D}]$, so that the estimated frequency response function represents closely the frequency response of the continuous state-space model determined by $[A, B, C, D]$.

In the electro-analytical method, measurement of the electrochemical cell’s response results in a set of magnitude ($Z(\omega_i)$) and phase ($\theta(\omega_i)$) measurements (i.e., $G(\omega_i)$), corresponding to the i th excitation signal applied frequency (ω_i). To ensure that a measured data set is sampled at a frequency above the Nyquist frequency to reproduce correctly the system dynamics, the sampling rate is adjusted to 10 times the applied frequency. A common approach to minimizing the L_2 -norm error is to minimize the least-squares cost function [29]:

$$\min_{\hat{A}, \hat{B}, \hat{C}, \hat{D}} \sum_{i=1}^l (W(\omega_i))^2 |\hat{G}(\omega_i) - F(\omega_i)|^2 \tag{6}$$

where $W(\omega_i)$ is the weight array, $F(\omega_i)$ is the measured data, $\hat{G}(\omega_i)$ is the estimated transfer function and l is the number of measurement data frequencies.

2.6. Estimation of Equivalent R-C Network Model

Once the state-space representation has been obtained, it is possible to estimate resistive-capacitive network arrays (Figure 5) or ladder networks. For instance, Saatci et al. used a similar approach to obtain lung RC networks from state-space representation of lung models [28]. To illustrate the process, consider the model of the electrochemical cell constructed using a set of Kelvin–Voigt elements [23,24].

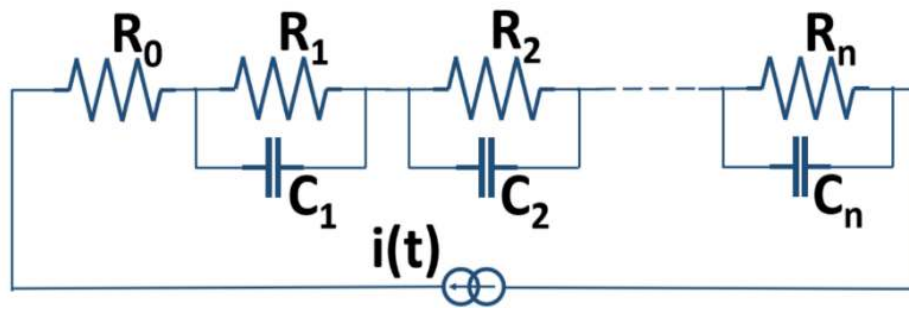


Figure 5. Modelling electrochemical cell using an array of Voigt elements plus a single resistor.

Assuming that the system’s poles are different from the system’s zeros and that $G(s)$:

$$G(s) = \frac{b_m s^m + b_{m-1} s^{m-1} + \dots + b_1 s + b_0}{s^n + a_{n-1} s^{n-1} + \dots + a_1 s + a_0} \tag{7}$$

which represents the model, is a proper rational function ($m \leq n$) corresponding to a linear, time-invariant, underdamped, stable system, the R-C network parameters can be deduced from the partial fraction expansion of $G(s)$.

Considering that the transfer function, $G(s)$, is the result of a combination of different first-order elements (i.e., Kelvin–Voigt-type element models as shown in Figure 4) and there are no repeated poles, $G(s)$, can be simplified to:

$$G(s) = \sum_{\Delta=0}^{m-n} d_{\Delta} s^{\Delta} + \sum_{\alpha=1}^n \frac{k_{\alpha}}{(s - P_{\alpha})} \tag{8}$$

where the coefficients k_{α} are calculated using the Heaviside cover-up method, as:

$$k_{\alpha} = \lim_{s \rightarrow P_{\alpha}} [(s - P_{\alpha}) G(s)] \quad \text{for } \alpha = 1, 2, \dots, n \tag{9}$$

The partial fraction expansion representation results in a summation of first-order functions, which for a proper function can be rewritten as:

$$G(s) = (d_0) + \frac{\left(\frac{k_1}{-P_1}\right)}{\left(\frac{s}{-P_1} + 1\right)} + \frac{\left(\frac{k_2}{-P_2}\right)}{\left(\frac{s}{-P_2} + 1\right)} + \frac{\left(\frac{k_3}{-P_3}\right)}{\left(\frac{s}{-P_3} + 1\right)} + \dots \tag{10}$$

Recalling Equation (4), the individual RC network parameters can be calculated as

$$C_{\alpha} = \left[\left[\frac{1}{k_{\alpha}}\right]\right]; R_{\alpha} = \left[\left[\frac{k_{\alpha}}{-P_{\alpha}}\right]\right]; R_0 = [d_0] \text{ for } \alpha = 1..n \tag{11}$$

Thus, the linear approximation of the electrochemical cell [20] can be represented as the network model as shown in Figure 5, using a combination of passive components.

2.7. Measurement Setup

Four commercial drugs were used in this experimental study. The EIS method was used to obtain a description of the impedance variations caused by the conductive properties of different compounds over the liquid test fixture operational frequency range (20 Hz to 30 MHz). The experimental setup is shown in Figure 6, which consists of three main components: (1) an impedance analyser with an operational frequency range from 20 Hz to 50 MHz (Keysight E4990A), (2) a liquid test fixture with an operational frequency range of 20 Hz to 30 MHz (Keysight 16452A) and (3) a 4-wire connection (Keysight 16048A).



Figure 6. Experimental array for measurements of electrical impedance of commercial drugs. Impedance analyser and Liquid Test Fixture schematic.

The specifications of the liquid test fixture (Figure 7) are:

- Electrode size: 38 ± 0.5 (mm) (circular geometry).
- Casing dimensions: 85 height \times 85 width \times 37 depth (mm).
- Materials (electrodes, spacers, liquid inlet and outlet): nickel-plated cobal (Fe 54%, Co 17%, Ni 29%).
- Insulator: ceramic insulator (alumina Al_2O_3).
- O-ring: Viton (Fluoro rubber).
- Insulator soldering: silver-copper and gold copper.

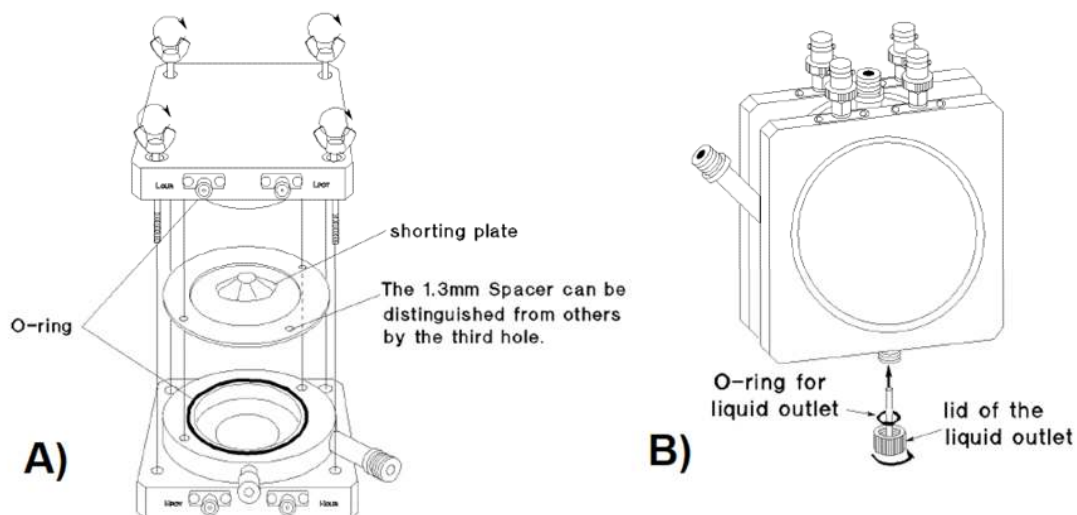


Figure 7. Keysight 16452A liquid test fixture. (A) Assembly detail (Short compensation) and (B) Assembled liquid test fixture. Reproduced with permission, courtesy of ©Keysight Technologies, Inc., 1994–2019.

The measurement equipment selected is an auto-balancing bridge, which offers the advantage of high accuracy over a wide impedance measurement range (20 Hz to 30 MHz), limited by the liquid test fixture operational frequency range [30]. This is well within the frequency range required to analyse the dielectric properties of the electrochemical cell filled with test samples. For every test, 200 impedance and phase data points, logarithmically separated over the measurement range, were obtained. The excitation voltage/current values were adjusted to $10 \text{ mV}_{\text{RMS}}/200 \mu\text{A}_{\text{RMS}}$.

Commercial drugs are often highly lipophilic and insoluble in aqueous media, materials frequently require the use of a solvent or carrier system to ensure adequate bioavailability. Thus, liquid crystals are a mixture of compounds in a state between liquid and solid forms [31]. Here, we used liquid-based drug suspensions, syrup and injectable solution ($C_{14}H_{18}N_4O_3$ - $C_{10}H_{11}N_3O_3$ Liomont Lab), ($C_{13}H_{18}Br_2N_2O.HCl$ Bruluart Lab), ($C_{13}H_{16}N_3NaO_4S$ SON'S Lab), and ($C_{13}H_{22}N_4O_3S.HCl$ PiSA Lab) of commercial-grade, respectively as listed in Table 2.

Table 2. Commercial drugs.

Trimethoprim/Sulfamethoxazole	Suspension
Oxolvan (Ambroxol)	Suspension
Magnil (Metamizole Sodium)	Syrup
Ranitidine	Injectable solution

The drugs were introduced in the test device using a syringe of 5 mL for each as shown in Figure 8.

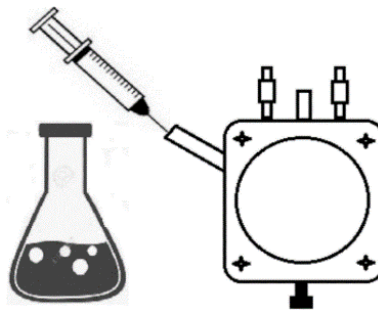


Figure 8. Schematic diagram of a commonly used impedance measurement Liquid Test fixture.

The measurement setup was 40 points per decade in a frequency range of 20 Hz to 30 MHz controlled signal. All tests were repeated twice to decrease the margin of measurement error for each test trial. The impedance measurement was made at 27 °C.

2.8. Determination of the Order Model

Appropriate determination of the model order is critical to obtain an accurate representation (fit) of measured data. It is often the case that trial-and-error is used to fit the model parameters, either by choosing a different combination of components or adding or subtracting components. Guascito et al. pointed out that blind fitting could lead to unsatisfactory results [32]. In frequency-domain identification, it is necessary to determine that the state-space model corresponds to the minimal realization. Saatci et al. considered the rank of observability and controllability matrices of lung models in correlation with the number of model states to assess the accuracy of linear respiratory models [28]. Another approach in frequency-domain modelling is to look at the Hankel singular values of the model including disturbances. Finally, the Akaike Information Criterion [33] derived from statistical model identification, is a measure of the fit of the model. We depart from the basic model configuration as shown in Figure 5 and then assess the validity of resulting models based on % fit, the rank of controllability and observability matrices, Hankel singular value and Akaike Information Criterion (AIC).

3. Results

The modelling procedure was implemented using MATLAB© (The MathWorks Inc., Natick, Massachusetts, USA, 2018) for matrix operations and statistical evaluation of the models and Excel© for graphs (Microsoft Corporation, 2018). Tables 3–6 show a comparison of model estimation for different numbers of parameters. Figure 9 shows a summary of the test results, comparing the approximations as described in Tables 3–6.

Table 3. Summary of model estimation for Metamizole Sodium.

Transfer function	Poles	2	3	3	4	4
	Zeroes	2	2	3	3	4
Electrical model	Number of model parameters	5	6	7	8	9
	Number of resistances	3	3	4	4	5
	Number of capacitors	2	3	3	4	4
Akaike information Criterion	% Fit	94.83	98.02	94.862	97.776	97.646
	Mean Squared Error (MSE)	1.016	0.15	1.005	0.1883	0.211
	Final Prediction Error (FPE)	1.042	0.1546	1.041	0.196	0.2206
	Number of samples	201	201	201	201	201
	AIC	1157	390.2	1157	485.6	533
	AICc	1157	390.5	1157	486	534
Controllability/ Observability analysis	Rank observability	2	3	3	1	1
	Unobservable states	0	0	0	3	3
	Rank controllability	2	1	3	1	1
	Uncontrollable states	0	2	0	3	3
	max log (Hankel SV)	7.61	16.52	*	*	*

* Uncontrollable state found.

Table 4. Summary of model estimation for Ambroxol.

Transfer Function	Poles	2	3	3	4	4
	Zeroes	2	2	3	3	4
Electrical Model	Number of Model Parameters	5	6	7	8	9
	Number of resistances	3	3	4	4	5
	Number of Capacitors	2	3	3	4	4
Akaike Information Criterion	% Fit	94.4	98.6	98	98.8	97.6
	Mean Squared Error (MSE)	1.569	0.094	0.2026	0.0776	0.297
	Final Prediction Error (FPE)	1.608	0.0968	0.2098	0.0808	0.3106
	Number of Samples	201	201	201	201	201
	AIC	1332	202.3	513.1	129.5	670.8
	AICc	1332	202.5	513.4	129.8	671.3
Controllability/ Observability Analysis	Rank Observability	2	3	3	1	4
	Unobservable States	0	0	0	3	0
	Rank Controllability	2	1	3	1	4
	Uncontrollable States	0	2	0	3	0
	max log (Hankel SV)	6.676	16.14	*	*	*

* Uncontrollable state found.

Table 5. Summary of model estimation for Trimethoprim/Sulfamethoxazole.

Transfer Function	Poles	2	3	3	4	4
	Zeroes	2	2	3	3	4
Electrical Model	Number of Model Parameters	5	6	7	8	9
	Number of resistances	3	3	4	4	5
	Number of Capacitors	2	3	3	4	4
Akaike Information Criterion	% Fit	93.11	97.69	97.37	97.73	97.76
	Mean Squared Error (MSE)	10.69	1.199	1.551	1.16	1.123
	Final Prediction Error (FPE)	10.96	1.235	1.606	1.207	1.175
	Number of Samples	201	201	201	201	201
	AIC	2103.427	1225.763	1331.341	1216.477	1205.560
	AICc	2103.578	1225.975	1331.626	1216.843	1206.020
Controllability/Observability Analysis	Rank Observability	2	3	3	3	1
	Unobservable States	0	0	0	1	3
	Rank Controllability	2	1	1	2	1
	Uncontrollable States	0	2	2	2	3
	max log (Hankel SV)	5.710	16.756	6.431	16.765	6.878

* Uncontrollable state found.

Table 6. Summary of model estimation for Ranitidine.

Transfer Function	Poles	2	3	3	4	4
	Zeroes	2	2	3	3	4
Electrical Model	Number of Model Parameters	5	6	7	8	9
	Number of resistances	3	3	4	4	5
	Number of Capacitors	2	3	3	4	4
Akaike Information Criterion	% Fit	90.15	90.15	97.09	99.65	99.65
	Mean Squared Error (MSE)	5.275	5.275	0.04882	0.006531	0.006531
	Final Prediction Error (FPE)	5.407	5.435	0.05087	0.006793	0.00683
	Number of Samples	201	201	201	201	201
	AIC	1819	1821	-48.12	-865.7	-863.7
	AICc	1819	1821	-47.78	-865.4	-863.3
Controllability/Observability Analysis	Rank Observability	2	3	3	1	1
	Unobservable States	0	0	0	3	3
	Rank Controllability	2	1	3	1	1
	Uncontrollable States	0	2	0	3	3
	max log (Hankel SV)	*	*	*	15.47	7.91

* Uncontrollable state found.

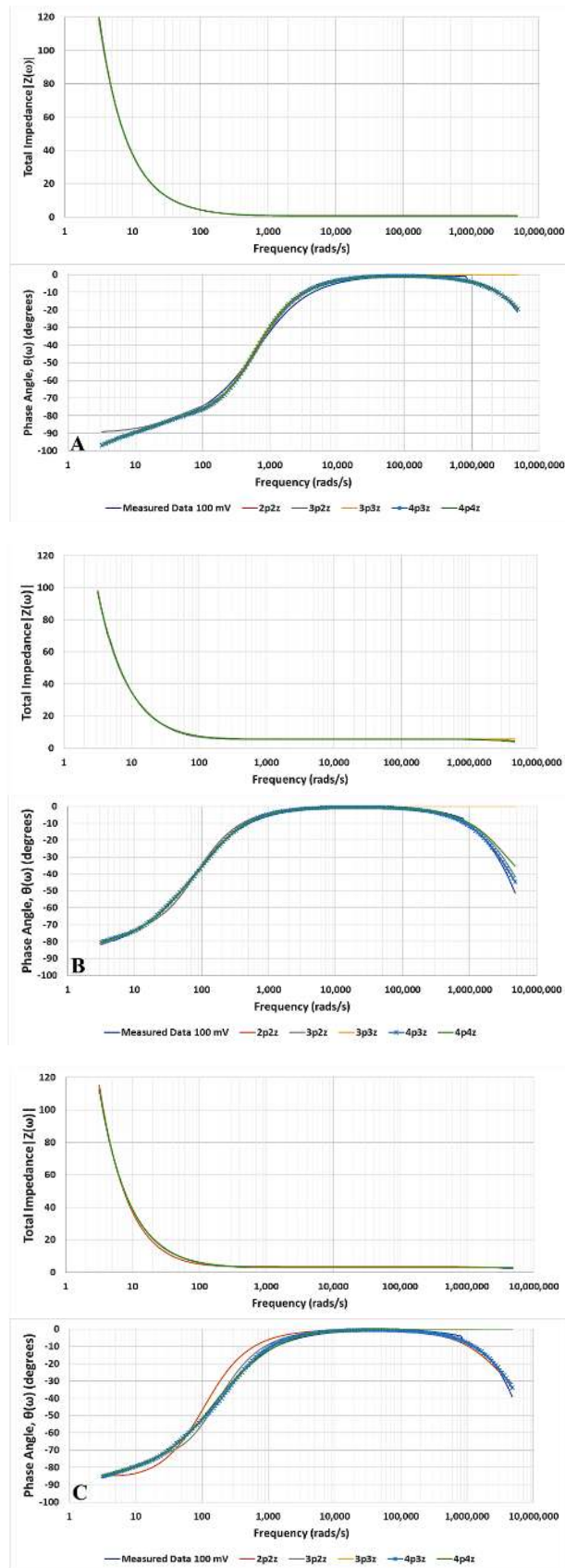


Figure 9. Cont.

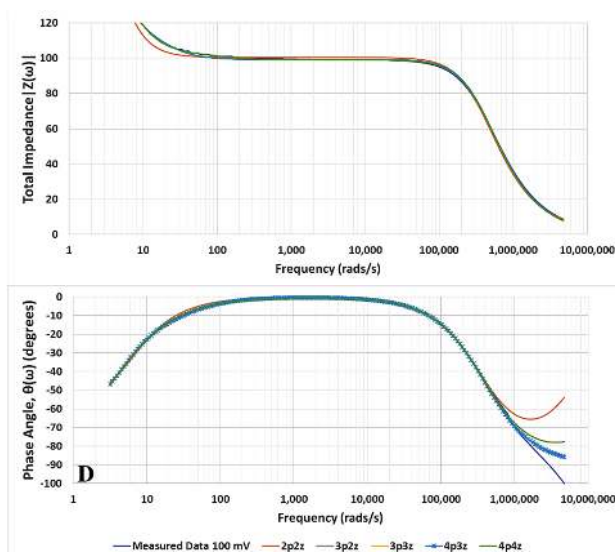


Figure 9. Summary of test results for (A) Ranitidine, (B) Metamizole, (C) Ambroxol, (D) Trimethoprim/Sulfamethoxazole and comparison with state-space fitting model derived from frequency-domain impedance data in the frequency range 20 Hz–30 MHz.

For a model to be a minimal state-space representation, the controllability analysis must result in zero unobservable and zero uncontrollable states and the Hankel singular value must be finite. Although all the models provide a reasonable approximation, only one estimation per experiment qualifies as a feasible representation. For instance, using six parameters to model metamizole provides a 98% approximation over the entire measurement frequency range. However, using six parameters does not represent a minimal state-space realization, since the Controllability/Observability analysis reveals two uncontrollable states. In the case of the seven-parameter model for ambroxol, the Controllability/Observability analysis reveals zero uncontrollable and zero unobservable states; however, the Hankel singular value is not finite and therefore does not correspond to a minimal state-space representation.

The values of the RC components for the four experiments are calculated in a similar manner for all four test samples as listed in Table 7. The best approximation is obtained for metamizole (94.93%) whereas the poorest approximation is obtained for ranitidine (90.15%). The 90.15% value is probably due to the error induced by a linear approximation to model the electrochemical cell, where only linear time-invariant components are used for modelling. In contrast, in Figure 9D, there appears to be a contribution of approximately -45° at low frequencies for trimethoprim/sulfamethoxazole which may be explained by a Warburg element.

Table 7. Summary of results: best feasible estimated electrochemical cell.

Electrical Component	Ranitidine	Metamizole	Ambroxol	Trimethoprim Sulfamethoxazole
	% Fit = 90.15	% Fit = 94.83	% Fit = 94.38	% Fit = 93.11
R_0 (Ω)	0.761	5.569	0.916	4.7
R_1 (Ω)	1.076	6.6	2.462	95.72
C_1 (F)	1.11×10^{-2}	1.1×10^{-2}	9.64×10^{-8}	2.9×10^{-8}
R_2 (Ω)	7.11×10^{12}	4072	1586	603.9
C_2 (F)	2.64×10^{-3}	3.28×10^{-3}	2.73×10^{-3}	2.24×10^{-3}

The importance of understanding the presence of CPE or Warburg impedance components has led to a wealth of rigorous mathematical descriptions in the literature. However, because this work is focused on the estimation of linear models, we consider constant phase elements being approximated

by a network of passive components [34]. In addition, the data considered for modelling comprise the range 20 Hz–30 MHz.

Identification of the Model Components

A wealth of methods has been proposed and reported to ease the identification of electrochemical processes from frequency response data, ranging from graphical analysis of Nyquist [35] and Bode diagrams [36] to multidimensional analysis [37] and software solutions [38]. There are indications that, over the last two decades [39], the trend in electrochemical sensing [40], measurement [41,42] and analysis has been directed towards real-time EIS analysis of dynamic systems. For instance, Lochner et al. [43] present an Impedance Real-Time Monitoring (IRTM) procedure for estimating Randles cell equivalent electrical circuits (EEC) of a polymer electrolyte fuel cell. Lochner et al. use five impedance measurements to obtain three sets of EEC parameters [43]; the authors reduce the time required for data acquisition and analysis by averaging the calculated EEC parameters, and claim that the IRTM procedure yields accuracies close to those obtained using iterative fitting procedures. The method presented here is directed towards obtaining a mathematically-derived indication that the EEC parameters represent the state-space model.

After the state-space model has been identified as a feasible state-space representation, the next step is to identify which component correlates to a particular electrochemical process. As a departure point, consider the transfer function of the resulting Trimethoprim/Sulfamethoxazole model in the frequency range 20 Hz–30 MHz:

$$G_{TRIM}(s) = \frac{1.765 \times 10^{-5} s^2 + 135.8 s + 704.3}{3.755 \times 10^{-6} s^2 + 1.353 s + 1} \quad (12)$$

which can be written in terms of DC Gain, poles and zeros as:

$$G_{TRIM}(s) = DC \text{ Gain} \left(\frac{\left(\frac{s}{Z_1} + 1\right)\left(\frac{s}{Z_2} + 1\right)}{\left(\frac{s}{P_1} + 1\right)\left(\frac{s}{P_2} + 1\right)} \right) \quad (13)$$

$$G_{TRIM}(s) = 3.1357 \times 10^{-2} \left(\frac{\left(\frac{s}{0.19286} + 1\right)\left(\frac{s}{1.30 \times 10^7} + 1\right)}{\left(\frac{s}{1.35281} + 1\right)\left(\frac{s}{2.78 \times 10^6} + 1\right)} \right) \quad (14)$$

The bode plot is the resulting effect (sum of the frequency response magnitude and frequency) of the five terms: DC Gain, Poles (P_1 , P_2) and Zeroes (Z_1 , Z_2). Figure 10 shows the resulting frequency response of each individual terms as well as that of the resulting bode plot of the complete model.

In order to ease the explanation of how each component relates to a particular electrochemical process, consider the Nyquist plot of the Trimethoprim/Sulfamethoxazole model (Figure 11).

In Figure 11, from left to right, the distance between the origin and the first semicircle corresponds to the bulk resistance, R_0 , consistent with the medium resistivity for the test conditions. The first semicircle from suggests that there is interfacial resistance originated by decomposition of the electrolyte, and corresponds to the effect of R_1 and C_1 , whereas the second semicircle represents the charge transfer resistance and double-layer capacitance (R_2 , C_2). For all drugs studied, increasing the number of parameters appears to yield an improved approximation. In contrast, the results indicate that a large number of equivalent electrical cells does not lead to a minimal realization of the state-space model. Thus, a five-element equivalent impedance model yields a reduced fit but corresponds to a minimal state-space realization. As for diffusion processes, which may drive the frequency response at low frequencies, a reduced number of equivalent model components seems to represent the process. In contrast, in ambroxol, there appears to be a physicochemical process, which may be described as a CPE that extends at higher frequencies; although a seven-parameter model appears to yield good approximation, the analysis of singular values indicates an uncontrollable state of the fitting

model and thus is not feasible linear time-invariant representation. Nevertheless, using a combination of five components can differentiate the frequency response of different medications. At present, the identification of different compounds can be carried out by comparison with a priori measurements. However, the wide range of EEC values and pattern combinations suggest that it is possible to use pattern identification methods to automate the identification of different compounds.

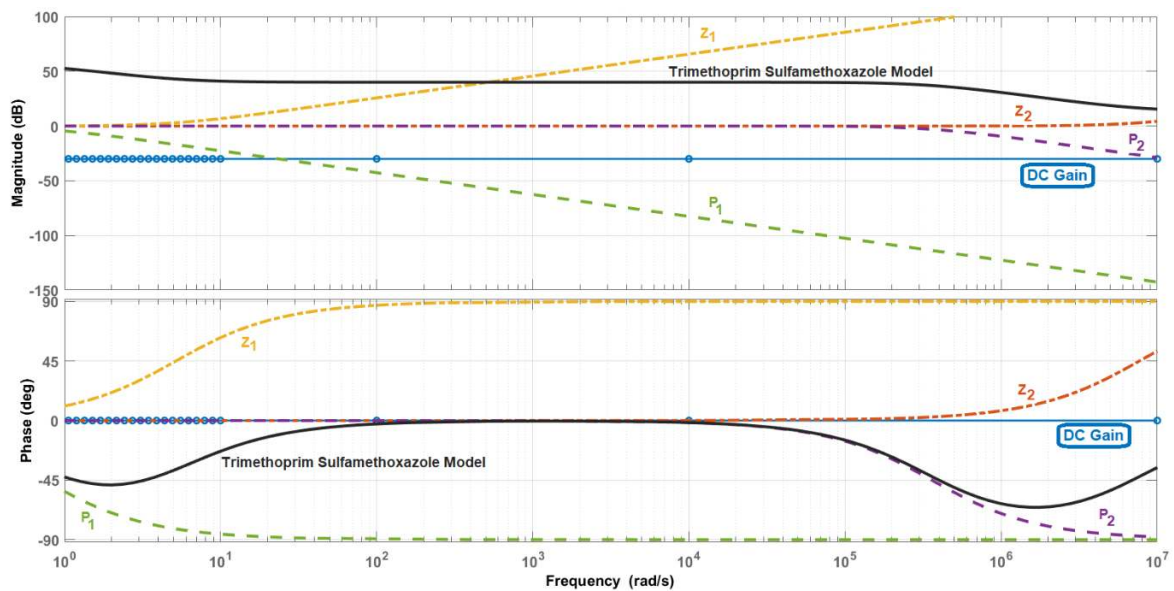


Figure 10. Bode plot of the Trimethoprim/Sulfamethoxazole model, showing the magnitude and phase contribution of each term.

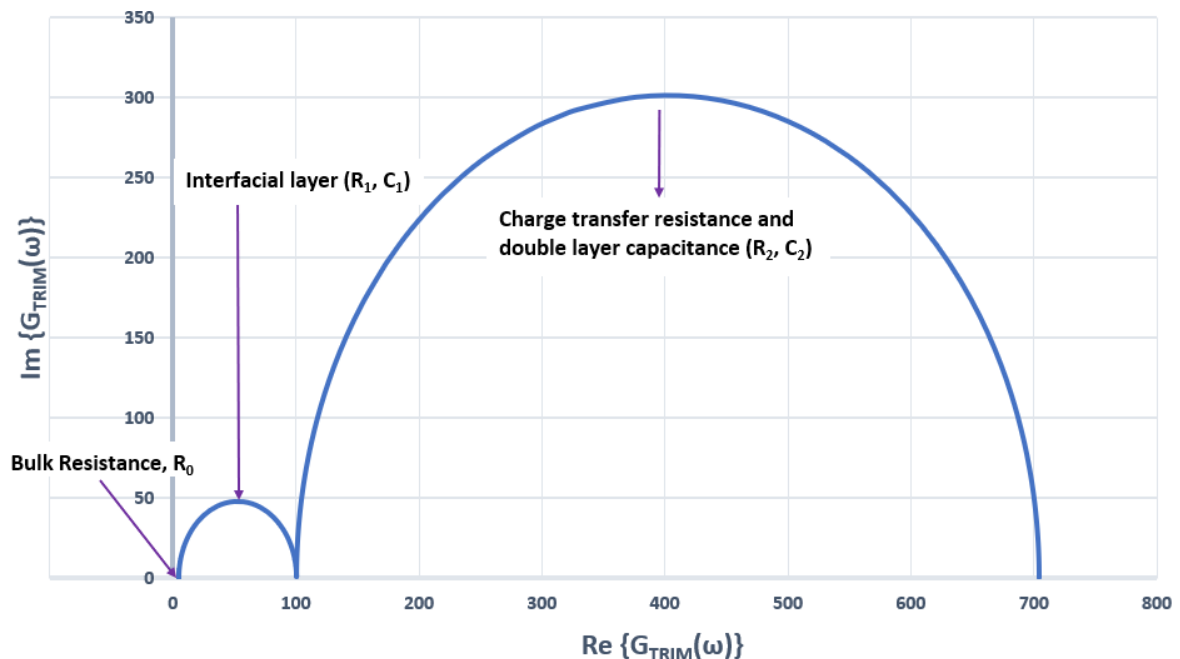


Figure 11. Nyquist diagram of the Trimethoprim/Sulfamethoxazole model.

4. Conclusions

Electrical Impedance Spectroscopy measurements were used to model the frequency response of four different drug compounds. Modelling was carried out using frequency-domain data to derive the equivalent electrical Kelvin–Voigt network models. The modelling process was evaluated by

comparing the percentage of fit, Akaike Information Criterion, rank of controllability and observability matrix and Hankel Singular values to determine if the model is a feasible representation of the resulting electrochemical process. The results indicate that although a higher fit can be obtained by increasing the number of components, the model may not be a minimal state-space representation. Thus, the limitation for the accurate modelling of an electrochemical process based on linear time-invariant equivalent electrical components is reflected. Nevertheless, based on the frequency response, a comparison of evaluation using a five-parameter model can be used to identify different drug compounds. In some cases, there appears to be a noticeable diffusion effect and thus the linear approximation induces errors, particularly at low frequencies, which are reflected in the % fit. Future work is directed to improving the modelling procedure to include non-linear effects and to correlate with the drug electrical impedance properties.

Author Contributions: Writing—original draft preparation, formal analysis M.V.-N. and J.-A.G.-G.; conceptualization, J.-A.G.-G.; funding acquisition, J.-A.G.-G.; investigation, E.R.-A.; methodology, W.Y.; validation, M.-A.R.-F.; visualization J.-C.O.-R. and D.L.-E. All authors have read and agreed to the published version of the manuscript.

Funding: The authors acknowledge the financial support of CONACYT under grant 1703 “Science Frontiers” and the financial support of Michoacán State’s Institute for Science, Technology and Innovation under grant CD-03/2019/04.

Conflicts of Interest: The authors declare no conflict of interest.

References

1. Siddiqui, M.R.; AlOthman, Z.A.; Rahman, N. Analytical techniques in pharmaceutical analysis: A review. *Arab. J. Chem.* **2017**, *10*, 1409–1421. [[CrossRef](#)]
2. Randviir, E.P.; Banks, C.E. Electrochemical impedance spectroscopy: An overview of bioanalytical applications. *Anal. Methods UK* **2013**, *5*, 1098–1149. [[CrossRef](#)]
3. Grossi, M.; Riccò, B. Electrical impedance spectroscopy (EIS) for biological analysis and food characterization: A review. *J. Sens. Sens. Syst.* **2017**, *6*, 303–325. [[CrossRef](#)]
4. Ragoisha, G.A. Challenge for electrochemical impedance spectroscopy in the dynamic world. *J. Solid State Electr.* **2020**, *24*, 2171–2172. [[CrossRef](#)]
5. Rimpiläinen, V.; Kuosmanen, M.; Ketolainen, J.; Järvinen, K.; Vauhkonen, M.; Heikkinen, L.M. Electrical impedance tomography for three-dimensional drug release monitoring. *Eur. J. Pharm. Sci.* **2010**, *41*, 407–413. [[CrossRef](#)]
6. Gabriel, C.; Gabriel, S.; Corthout, E. The dielectric properties of biological tissues: I. Literature survey. *Phys. Med. Biol.* **1996**, *41*, 2231–2249. [[CrossRef](#)]
7. Gabriel, S.; Lau, R.W.; Gabriel, C. The dielectric properties of biological tissues: II. Measurements in the frequency range 10 Hz to 20 GHz. *Phys. Med. Biol.* **1996**, *41*, 2251–2269. [[CrossRef](#)]
8. Gabriel, S.; Lau, R.W.; Gabriel, C. The dielectric properties of biological tissues: III. Parametric models for the dielectric spectrum of tissues. *Phys. Med. Biol.* **1996**, *41*, 2271–2293. [[CrossRef](#)]
9. Clemente, F.; Arpaia, P.; Manna, C. Characterization of human skin impedance after electrical treatment for transdermal drug delivery. *Measurement* **2013**, *46*, 3494–3501. [[CrossRef](#)]
10. Grossi, M.; Parolin, C.; Vitali, B.; Riccò, B. Electrical Impedance Spectroscopy (EIS) Characterization of saline solutions with a low-cost portable measurement system. *Eng. Sci. Technol.* **2019**, *22*, 102–108. [[CrossRef](#)]
11. Keysight Technologies. *A Guide to Measurement Technology and Techniques*, 6th ed.; Impedance Measurement Handbook. Document 5950–3000. Available online: <https://www.keysight.com/us/en/assets/7018-06840/application-notes/5950-3000.pdf> (accessed on 10 July 2020).
12. Newman, J. Resistance for flow of current to a disk. *J. Electrochem. Soc.* **1966**, *113*, 501–502. [[CrossRef](#)]
13. Newman, J. Frequency dispersion in capacity measurements at a disk electrode. *J. Electrochem. Soc.* **1970**, *117*, 198–203. [[CrossRef](#)]
14. Davis, K.; Dizon, A.; Alexander, C.L.; Orazem, M.E. Influence of geometry-induced frequency dispersion on the impedance of rectangular electrodes. *Electrochim. Acta* **2018**, *283*, 1820–1828. [[CrossRef](#)]

15. Gharbi, O.; Dizon, A.; Orazem, M.E.; Tran, M.T.T.; Tribollet, B.; Vivier, V. From frequency dispersion to Ohmic impedance: A new insight on the high-frequency impedance analysis of electrochemical systems. *Electrochim. Acta* **2019**, *320*, 134609. [CrossRef]
16. Levent, A.; Yardim, Y.; Şentürk, Z. Electrochemical performance of boron-doped diamond electrode in surfactant-containing media for ambroxol determination. *Sens. Actuators B-Chem.* **2014**, *203*, 517–526. [CrossRef]
17. Yari, A.; Shams, A. Silver-filled MWCNT nanocomposite as a sensing element for voltammetric determination of sulfamethoxazole. *Anal. Chim. Acta* **2018**, *1039*, 51–58. [CrossRef]
18. Sgobbi, F.L.; Razzino, A.C.; Machado, A.S. A disposable electrochemical sensor for simultaneous detection of sulfamethoxazole and trimethoprim antibiotics in urine based on multiwalled nanotubes decorated with Prussian blue nanocubes modified screen-printed electrode. *Electrochim. Acta* **2016**, *191*, 1010–1017. [CrossRef]
19. Chen, C.; Chen, C.Y.; Hong, T.Y.; Lee, W.T.; Huang, F.J. Facile fabrication of ascorbic acid reduced graphene oxide-modified electrodes toward electroanalytical determination of sulfamethoxazole in aqueous environments. *Chem. Eng. J.* **2018**, *352*, 188–197. [CrossRef]
20. Gamry Instruments, Basics of Electrochemical Impedance (Application Note). Available online: <https://www.gamry.com/application-notes/EIS/basics-of-electrochemical-impedance-spectroscopy/> (accessed on 10 July 2020).
21. Sindhuja, M.; Kumar, N.S.; Sudha, V.; Harinipriya, S. Equivalent circuit modeling of microbial fuel cells using impedance spectroscopy. *J. Energy Storage* **2016**, *7*, 136–146. [CrossRef]
22. Ahmad, Z.; Mishra, A.; Abdulrahim, S.M.; Touati, F. Electrical equivalent circuit (EEC) based impedance spectroscopy analysis of HTM free perovskite solar cells. *J. Electroanal. Chem.* **2020**, *871*, 114294. [CrossRef]
23. Liao, H.; Watson, W.; Dizon, A.; Tribollet, B.; Vivier, V.; Orazem, M.E. Physical properties obtained from measurement model analysis of impedance measurements. *Electrochim. Acta* **2020**, *354*, 136747. [CrossRef]
24. Agarwal, P.; Orazem, M.E.; Garcia-Rubio, L.H. Measurement models for electrochemical impedance spectroscopy I. Demonstration of Applicability. *J. Electrochem. Soc.* **1992**, *139*, 1917–1927. [CrossRef]
25. Pavel, C.; Przemyslaw, D. Electrochemical Impedance Spectroscopy as a tool for electrochemical rate constant estimation. *J. Vis. Exp.* **2018**, *140*, 56611.
26. Ramos-Barrado, J.R.; Montenegro, G.P.; Cambon, C.C. A generalized Warburg Impedance for a nonvanishing relaxation process. *J. Chem. Phys.* **1996**, *105*, 2813. [CrossRef]
27. Huang, J. Diffusion impedance of electroactive materials, electrolytic solutions and porous electrodes: Warburg impedance and beyond. *Electrochim. Acta* **2018**, *281*, 170–188. [CrossRef]
28. Saatci, E.; Saatci, E.; Akan, A. Analysis of linear lung models based on state-space models. *Comput. Methods Prog. Biomed.* **2020**, *183*, 105094. [CrossRef]
29. Chen, C.W.; Juang, J.N.; Lee, G. Frequency Domain State-Space System Identification. In Proceedings of the 1993 American Control Conference, American Automatic Control Council, San Francisco, CA, USA, 2–4 June 1993; pp. 3057–3061. [CrossRef]
30. Keysight Technologies. Keysight 16452A Liquid Test Fixture, Operation and Service Manual. Document 16452–90000. Available online: <https://www.keysight.com> (accessed on 10 July 2020).
31. Chuealee, R.; Aramwit, P.; Srichana, T. Characteristics of cholesteryl cetyl carbonate liquid crystals as drug delivery systems. In Proceedings of the 2nd IEEE International Conference on Nano/Micro Engineered and Molecular Systems, Bangkok, Thailand, 16–19 January 2007; pp. 1098–1103.
32. Guascito, M.R.; Alfinito, E.; Cataldo, R.; Giotta, L. Tips for a (simple) Interpretation of the impedance response of an electrochemical cell. *IEEE Sens. J.* **2019**, *19*, 11318–11322. [CrossRef]
33. Akaike, H. A new look at the statistical model identification. *IEEE T. Automat. Control* **1974**, *19*, 716–723. [CrossRef]
34. Valsa, J.; Dvořák, P.; Friedl, M. Network model of the CPE. *Radioengineering* **2011**, *20*, 619–626.
35. Schwake, A.; Geuking, H.; Cammann, K. Application of a new graphical fitting approach for data analysis in electrochemical impedance spectroscopy. *Electroanalysis* **1999**, *10*, 1026–1029. [CrossRef]
36. Huang, J.; Li, Z.; Liaw, B.Y.; Zhang, J. Graphical analysis of electrochemical impedance spectroscopy data in Bode and Nyquist representations. *J. Power Sources* **2016**, *309*, 82–98. [CrossRef]
37. Ragoisha, G.A.; Bondarenko, A.S. Potentiodynamic electrochemical impedance spectroscopy. *Electrochim. Acta* **2005**, *50*, 1553–1563. [CrossRef]

38. Bodarenko, A.S.; Ragoisha, G.A. Inverse problem in potentiodynamic electrochemical impedance spectroscopy. In *Chapter 7 in Progress in Chemometrics Research*; Pomerantsev, A.L., Ed.; Nova Science: New York, NY, USA, 2005; pp. 89–102.
39. Wang, J. Real-time electrochemical monitoring: Toward green analytical chemistry. *Acc. Chem. Res.* **2002**, *35*, 811–816. [[CrossRef](#)] [[PubMed](#)]
40. Mishra, R.K.; Nunes, G.S.; Souto, L.; Marty, J.L. Screen printed technology—An application towards biosensor development. In *Encyclopedia of Interfacial Chemistry*; Klaus, W., Ed.; Elsevier: Amsterdam, The Netherlands, 2018; pp. 487–498.
41. Mora, L.; Chumbimuni-Torres, K.Y.; Clawson, C.; Hernandez, L.; Zhang, L.; Wang, J. Real-time electrochemical monitoring of drug release from therapeutic nanoparticles. *J. Control. Release* **2009**, *140*, 69–73. [[CrossRef](#)] [[PubMed](#)]
42. Alizadeh, N.; Shamaeli, E.; Fazili, M. Online spectroscopic monitoring of drug release kinetics from nanostructured dual-stimuli-responsive conducting polymer. *Pharm. Res.* **2017**, *34*, 113–120. [[CrossRef](#)]
43. Lochner, T.; Perchthaler, M.; Binder, J.T.; Sabawa, J.P.; Dao, T.A.; Bandarenka, A.S. Real-time impedance analysis for the on-road monitoring of automotive fuel cells. *Chem. Eur. Soc. Publ.* **2020**, *7*, 2784–2791.



© 2020 by the authors. Licensee MDPI, Basel, Switzerland. This article is an open access article distributed under the terms and conditions of the Creative Commons Attribution (CC BY) license (<http://creativecommons.org/licenses/by/4.0/>).